SOME TRANSVERSE RESONANT VIBRATION CHARACTERISTICS OF WIRE ROPE WITH APPLICATION TO FLOW-INDUCED CABLE VIBRATIONS

S. E. Ramberg, et al

Naval Research Laboratory
Washington, D. C.

10 December 1974

SECURITY CLASSIFICATION OF THIS PAGE (When Data Entered)

REPORT DOCUMENTATION PAGE

READ INSTRUCTIONS BEFORE COMPLETING FORM

1 REPORT NUMBER: NRL Report 7821

2. GOVT ACCESSION NO.

3. RECIPIENT'S CATALOG NUMBER: AD/A-000926

4 TITLE (and Subtitle): SOME TRANSVERSE RESONANT VIBRATION CHARACTERISTICS OF WIRE ROPE WITH APPLICATION TO FLOW-INDUCED CABLE VIBRATIONS

5. TYPE OF REPORT & PERIOD COVERED: Final report on one phase of a continuing program.

6. PERFORMING ORG. REPORT NUMBER

7. AUTHOR(s): S.E. Ramberg and O.M. Griffin

8. CONTRACT OR GRANT NUMBER(s)

9 PERFORMING ORGANIZATION NAME AND ADDRESS: Naval Research Laboratory, Washington, D.C. 20375

10. PROGRAM ELEMENT, PROJECT, TASK AREA & WORK UNIT NUMBERS: NRL Prob F02-36.401; Proj. PO-4-0009(PDM-03)

11. CONTROLLING OFFICE NAME AND ADDRESS: Department of the Navy, Naval Facilities Engineering Command, Alexandria, Virginia 22332

12. REPORT DATE: December 10, 1974

13. NUMBER OF PAGES: 23

14 MONITORING AGENCY NAME & ADDRESS (if different from Controlling Office)

15. SECURITY CLASS. (of this report): Unclassified

15a. DECLASSIFICATION/DOWNGRADING SCHEDULE

16. DISTRIBUTION STATEMENT (of this Report)

Approved for public release; distribution unlimited.

17. DISTRIBUTION STATEMENT (of the abstract entered in Block 20, if different from Report)

18. SUPPLEMENTARY NOTES

19. KEY WORDS (Continue on reverse side if necessary and identify by block number)

Flow-induced cable vibrations
Cable strumming
Cable damping
Submerged moorings
Vortex shedding
Ocean engineering

20. ABSTRACT (Continue on reverse side if necessary and identify by block number)

The transverse resonant vibration of stranded wire rope was studied as part of an overall investigation of flow-induced cable vibrations. It was found that an equivalent homogeneous string model adequately predicts the cable resonant frequencies. Furthermore, the in-water damping and added mass exhibit no dependence on amplitude, mode shape, or wavelength, and the frequency dependence is slight. The measured damping and added mass were combined to form a stability parameter which can be used to correctly estimate the maximum amplitude of the transverse vibrations induced by the interaction between a steady current and an elastic or elastically-mounted structure.

DD FORM 1 JAN 73 1473 EDITION OF 1 NOV 65 IS OBSOLETE
S/N 0102-014-6601

SECURITY CLASSIFICATION OF THIS PAGE (When Data Entered)

CONTENTS

SOME TRANSVERSE RESONANT VIBRATION CHARACTERISTICS OF WIRE ROPE WITH APPLICATION TO FLOW-INDUCED CABLE VIBRATIONS

INTRODUCTION AND RELATED INVESTIGATIONS

The increased use in marine construction of light structural elements with little damping has resulted in the more frequent occurrence of undesirable vibrations. Wire rope, one of the most widely used marine structural elements of this type, is particularly susceptible to vibration since its bluff shape can experience alternating transverse forces when a current flows about the cable and produces alternate shedding of vortices. Furthermore, at a coincidence of the vortex shedding frequency and a cable resonant frequency, large transverse motions often take place. The authors have recently examined the flow about a resonantly vibrating cable [1, 2] to relate the properties of the wake to the cable motion and to the existing information on the flow-induced forces. These investigations have indicated that a cable strumming model can be developed as an extension of NRL's successful wake-oscillator model [3] for predicting the vortex-excited oscillations of elastically mounted, rigid structures.

Some knowledge of the resonance characteristics of wire rope is required in order to establish an adequate predictive model for these flow-induced cable vibrations. The purpose of this report is to examine the resonant behavior of wire rope to determine a satisfactory governing equation for the cable motion and to ascertain the cable damping and added mass in water. These quantities are combined to form a cable strumming stability parameter that is analogous to the results with the aforementioned wake-oscillator model.

Wire rope, considered as a structural element, presents the analyst with a complex internal construction that varies considerably in the number, arrangement, and material of individual strands. Because of this difficulty, and because wire r is generally quite flexible, previous investigators [4, 5] have concluded that the transverse vibration of a cable is primarily controlled by the steady-state, or static, tension. The cable motion is then governed by the linear wave equation for an equivalent homogeneous string. More recently, Heller and Chung [6] included the effect of cable bending stiffness by modeling the cable as an axially loaded, Bernoulli-Euler beam. Their experiments for a variety of wire ropes in a fundamental mode indicated that the equivalent homogeneous string was an adequate representation of vibrating wire rope for their experimental conditions. Both theoretical treatments are linear, i.e., small displacements are assumed, and from the description of Heller and Chung's experimental procedures it can be inferred that the experimental peak-to-peak amplitudes never exceeded 30% of a cable diameter and were generally smaller [7].

This raises a question concerning the magnitude of nonlinear effects during flow-induced cable vibrations when amplitudes between 10 and 100% of a diameter are known to occur. It is also of practical importance to know the resonant behavior of such properties

Manuscript submitted September 4, 1974.

as the cable damping and added mass, and how they are related to mode shape, wavelength, and tension as well as to amplitude. None of this information was available before the initiation of the present study.

EXPERIMENTAL SYSTEMS AND METHODS

The wire rope specimens were mounted in either of two aluminum frames (Figs. 1, 2) that applied an axial load to the cable while providing the desired boundary conditions at known locations. The major differences between the two frames were the load ranges obtained, the lengths of the specimens, and the end conditions. The shorter frame had a higher load capacity and provided clamped end conditions, whereas the longer frame had a low load capacity and provided pinned end conditions. The load was measured by a transducer located at one end of the cable. The driving force for the cable motion was obtained by placing electromagnetic transducers along the cable at locations favorable to the desired mode of vibration. These electromagnets were driven by two power amplifiers and a common signal generator that adjusted the relative phasing between amplifiers according to the transducer location and the desired mode.

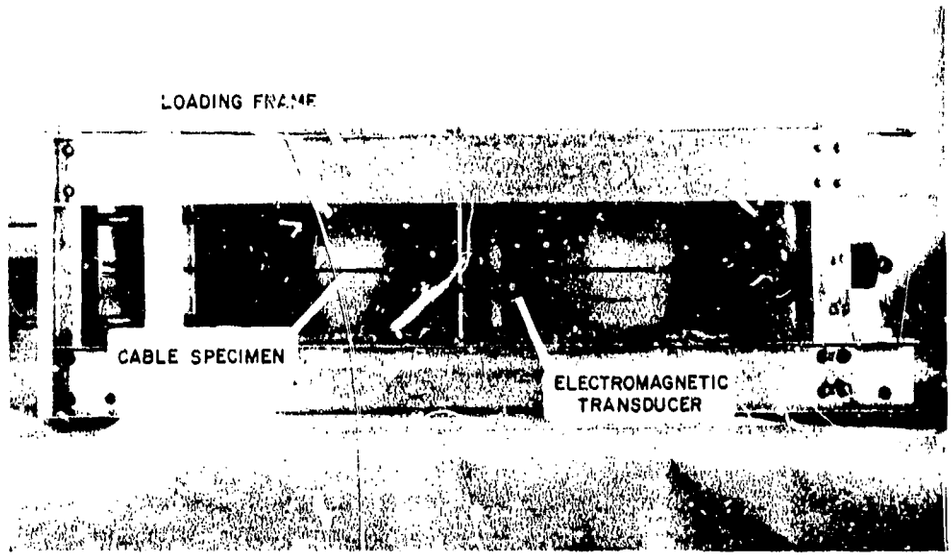

Fig. 1 — Loading frame (5 ft)

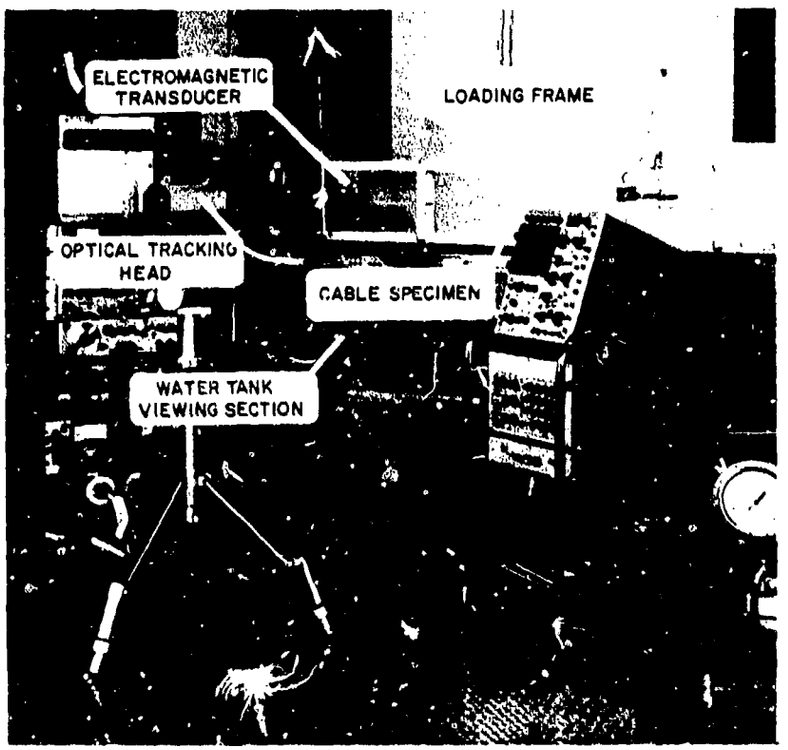

Fig. 5 — Loading frame (15 ft) and water tank

The motion of the cable was detected by backlighting the cable and optically tracking the displacement with a Physitech 440 autocollimator. The driving and measuring systems were thus independent and the amplitude could be measured accurately. The motion signal from the autocollimator was viewed on an oscilloscope, and resonant frequencies were determined by observing the frequency at which the maximum amplitude occurred at each load condition. Once a steady state resonant condition was established, the driving forces were disconnected and the decay of the free vibration was recorded to obtain a measure of the damping. For frequencies greater than 15 Hz, the decaying signal was processed in a log converter and plotted on a chart recorder; the damping was determined from the slope of the printed record. For frequencies below 15 Hz, the actual transient signal was recorded on an oscilloscope screen and photographed. The log decrement was calculated from measurements on the photograph according to

$$\delta = ln \frac{y_n}{y_{n+1}},$$

in which y_n and y_{n+1} are amplitudes of successive peaks of the decaying signal. These experiments were performed both in air and in water to deduce the effect of water mass loading. After several runs the in-air damping measurements were discontinued for reasons discussed in the next section.

The added mass effect due to the motion of the surrounding fluid is customarily treated as proportional, by the added mass coefficient K, to the mass of the fluid displaced by the body. Therefore, the ratio of virtual mass density in water to the body's mass density in air is given by

$$\frac{\rho_W}{\rho_A} = 1 + \frac{K}{S} \tag{1}$$

in which S is the specific gravity of the wire rope. It is assumed that the fluid loading in air is negligible. In addition, the ratio of the in-air resonant frequency f_A to the in-water resonant frequency f_W at the same load and mode shape is given by (using the string approximation)

$$\frac{f_A}{f_W} = \left(\frac{\rho_W}{\rho_A}\right)^{1/2} \tag{2}$$

The added mass coefficient is determined from experimental results by means of Eqs. (1) and (2) which combine to give

$$K = S \left| \left(\frac{f_A}{f_W}\right)^2 - 1 \right|. \tag{3}$$

Since f_A and f_W are usually close, particularly at low frequencies, a small error (1 or 2%) in one or both can result in relatively large variations in K (about 10 to 40%). For this reason it is helpful to also consider the ratio of virtual to actual mass which, according to Eq. (2), is the square of the frequency ratio f_A/f_W. Most of the conclusions in this study regarding the added mass effect are based on the measured values of f_A/f_W.

EQUATION OF MOTION FOR A STRETCHED CABLE

Consider a uniform cable stretched between rigid supports a distance L apart with an equilibrium position along the x axis and equilibrium tension T_0 (Fig. 3). The cable has a virtual mass density ρ, cross-sectional area A, elastic modulus E, and a moment of inertia I about the neutral axis z; it experiences transverse oscillations only in the xy plane. To account for the damping, we assume a term in the equation linearly proportional to the transverse velocity by a damping coefficient β. The coefficient β is taken as the damping of the system as measured in a stationary fluid of the same properties as the flowing fluid. That is, β represents the sum of structural, fluid, and externally applied damping as appropriate. Longitudinal displacements are neglected and the transverse displacement at the position x is taken to be $\eta(x,t)$. Further, for typical cables and the frequencies of flow-induced vibrations, shear deformations and rotary inertia are negligible. The potential energy of the cable is then a sum of bending and stretching potential energies. From elementary beam theory the bending energy is given by

$$\int_0^L \tfrac{1}{2} EI \frac{\partial^2 \eta}{\partial x^2} \, dx. \tag{4}$$

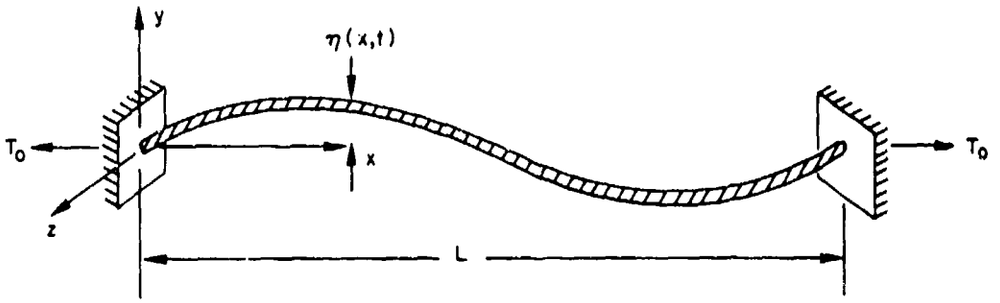

Fig. 3 — A cable in the second mode

We will use the approach developed by Murthy and Ramakrishna [8] to determine the stretching contribution for the nonlinear vibrations of strings. The development is identical to the original except that the cable is limited to planar motion. This is a good approximation for cables that undergo flow-induced "strumming" motions in water. As an element of cable dx is deformed into the planar element ds, the stretched length of the element is

$$ds = (dx^2 + dy^2)^{1/2} = dx \left[1 + \left(\frac{\partial \eta}{\partial x} \right)^2 \right]^{1/2} \tag{5}$$

and the local strain is given by

$$\epsilon = \frac{ds - dx}{dx} \simeq \left[1 + \left(\frac{\partial \eta}{\partial x} \right)^2 \right]^{1/2} \quad 1. \tag{6}$$

If the amplitudes are small enough for Hooke's law to be valid, then the local tension is

$$T = T_0 + EA\epsilon \tag{7}$$

and the local potential energy is equal to the product of the average local tension and the local stretching. Expanding the local strain in a power series of $\partial\eta/\partial x$ and neglecting terms higher than fourth order results in

$$\left[\tfrac{1}{2} T_0 \left(\frac{\partial \eta}{\partial x} \right)^2 + \frac{EA - T_0}{8} \left(\frac{\partial \eta}{\partial x} \right)^4 \right] dx, \tag{8}$$

the local potential energy due to stretching. For all practical cases $EA \gg T_0$ and the contribution to potential energy from stretching is

$$\int_0^L \left[\tfrac{1}{2} T_0 \left(\frac{\partial \eta}{\partial x} \right)^2 + \frac{EA}{8} \left(\frac{\partial \eta}{\partial x} \right)^4 \right] dx. \tag{9}$$

The kinetic energy of the cable is given by

$$\int_0^L \tfrac{1}{2}\rho_A \left(\frac{\partial \eta}{\partial t}\right)^2 dx \tag{10}$$

and the generalized work due to damping per unit length is

$$\int_0^L \beta \frac{\partial \eta}{\partial t}\,\delta\eta\, dx. \tag{11}$$

After Hamilton's principle is applied, the final equation of planar cable motion becomes

$$EI\frac{\partial^4 \eta}{\partial x^4} + \rho A \frac{\partial^2 \eta}{\partial t^2} \left| T_0 + \frac{3EA}{2}\left(\frac{\partial \eta}{\partial x}\right)^2 \right| \frac{\partial^2 \eta}{\partial x^2} + \beta \frac{\partial \eta}{\partial t} = 0. \tag{12}$$

It is convenient to transform this equation by

$$\dot{x} = \frac{N\pi x}{L}, \quad \dot{\eta} = \frac{\eta}{a}, \quad \dot{t} = \omega t \tag{13}$$

where N is the mode number, a is the antinode amplitude, and ω is the frequency of vibration. The resulting equation is

$$\frac{\partial^2 \dot{\eta}}{\partial \dot{t}^2} + \frac{EIN^4\pi^4}{\rho A \omega^2 L^4}\frac{\partial^4 \dot{\eta}}{\partial \dot{x}^4} \left| \frac{T_0 N^2\pi^2}{\rho A L^2 \omega^2} + \frac{3Ea^2N^4\pi^4}{2\rho\omega^2 L^4}\left(\frac{\partial \dot{\eta}}{\partial \dot{x}}\right)^2 \right| \frac{\partial^2 \dot{\eta}}{\partial \dot{x}^2} + \frac{\delta}{2\pi}\frac{\partial \dot{\eta}}{\partial \dot{t}} = 0, \tag{14}$$

in which δ is the log decrement of the vibration.

Consider the ratio of the fluctuating tension to the equilibrium tension,

$$\frac{3}{2}\frac{EA}{T_0}\frac{a^2}{L^2}N^2\pi^2.$$

It is reasonable to assume that $EA/T_0 = E/\sigma \approx 6 \times 10^3$ and a $\approx D/2$ for actual cables that undergo flow-induced vibration. Furthermore $L/D \approx 10^3$ is a conservative estimate, particularly for $N > 2$, and the ratio thus becomes proportional to $N^2 \times 10^{-1}$. With these estimates and the additional fact that $I \approx (D/2)^4$, one finds that the ratio of bending stiffness to equilibrium tension is on the order of $N^2 \times 10^{-2}$. The justification for treating the cable as an equivalent homogeneous string is thus apparent, as well as an ordering of the assumptions inherent in this approximation. Since the nonlinearity is small, a first approximation to the nonlinear tension fluctuation T_f can be obtained by substituting the linear string equation solution into that term, which yields the result

$$T_f = \frac{3\pi^2 a^2 N^2 EA}{2L^2}\cos^2\frac{N\pi x}{L}\sin^2\omega t. \tag{15}$$

The motion of a particular cable can now be adequately predicted if the required properties are known. The virtual mass and damping are not readily available, so that the experimental determination of these parameters is required.

SCOPE OF EXPERIMENTAL PROGRAM

The enormous variety of commercially available wire ropes precludes a generalization of resonant properties from tests of a few specimens, and also renders a test of all or most types a tedious task. Nevertheless, for the variety of 3/8 in. diameter cables tested by Heller and Chung [6], the added mass exhibited a general behavior, whereas the variation in damping (within one medium) was less than an order of magnitude. Some trends did appear according to material and type of construction. During the formulation of this investigation the authors decided not to test a wide variety of construction types but rather to study extensively several samples of similar construction under more varied conditions. In this way more parameters of practical importance were examined and the results generalized for other constructions within the limits cited above. Of additional practical importance are low frequency measurements (less than 20 Hz) and low tension measurements (loads less than 10% of the rupture strength) up to and including "slack" cables. Table 1 lists the ranges and types of experimental conditions employed in this study. Although the parameter ranges are not independent, i.e. low tension plus long wavelengths results in low frequencies, the overlap of experimental conditions and the insensitivity of the cable behavior to changes in some parameters allowed the data to be reduced easily.

RESONANT FREQUENCIES AND ADDED MASS

The measured resonant frequency as a function of tension is plotted for each configuration in Figs. 4 and 5. Figure 4 presents the resonant frequency measurements for a 1/4 in. diameter specimen in a fundamental mode at three nominal lengths of 5, 9, and 13 ft. Also shown are measurements of the second mode frequency for a length of 5 ft. The predicted homogeneous string resonant frequency is presented in each case for comparison. Fig. 5 contains the measured and predicted resonant frequencies of a 3/32 in. diameter specimen for a 15-ft length in the first three modes. The changes in specimen length or mode shape result in effective wavelength ranges for the two figures of 5 to 26 ft and 9.6 to 29 ft, respectively. Aside from the general agreement with the predicted frequency, two other observations can be made. First, changes in resonant frequency in *both* air and water due to various specimen lengths and modes are — to a good approximation — linearly related to ratios of specimen lengths or mode numbers. This implies that the added mass is independent, or nearly so, of mode shape and wavelength. Second, the essentially equivalent added mass effect at various modes requires the fluid loading to be also independent, or nearly so, of frequency.

Table 1
Range of Parameters

Cable	Nominal Length (ft)	Mode Numbers	Tension (% Rupture)	Wavelength / Diameter	Frequency (Hz)	Reynolds Number $\left(\frac{D^2\omega}{4\nu}\right)$	Amplitude / Diameter
1/4 in. diam 6 × 19 preformed improved plowsteel	5	1,2	1.5 – 30	40,20	17 – 130	1050 – 8060	0.5
	9	1	1.5 – 10	72	10 – 22	620 – 1360	
	13	1	1.5 – 10	104	7 – 17	430 – 1050	
3/32 in. diam 7 × 19 S.S. aircraft cable	15	1,2,3	1 – 25	309 – 103	3 – 55	26 – 480	0 – 1.0
3/8 in. diam {6 × 19 / 17 × 19}*	5	1	15 – 60	26.7	20 – 120	2780 – 16700	0 – .3

*Data from Ref. 9.

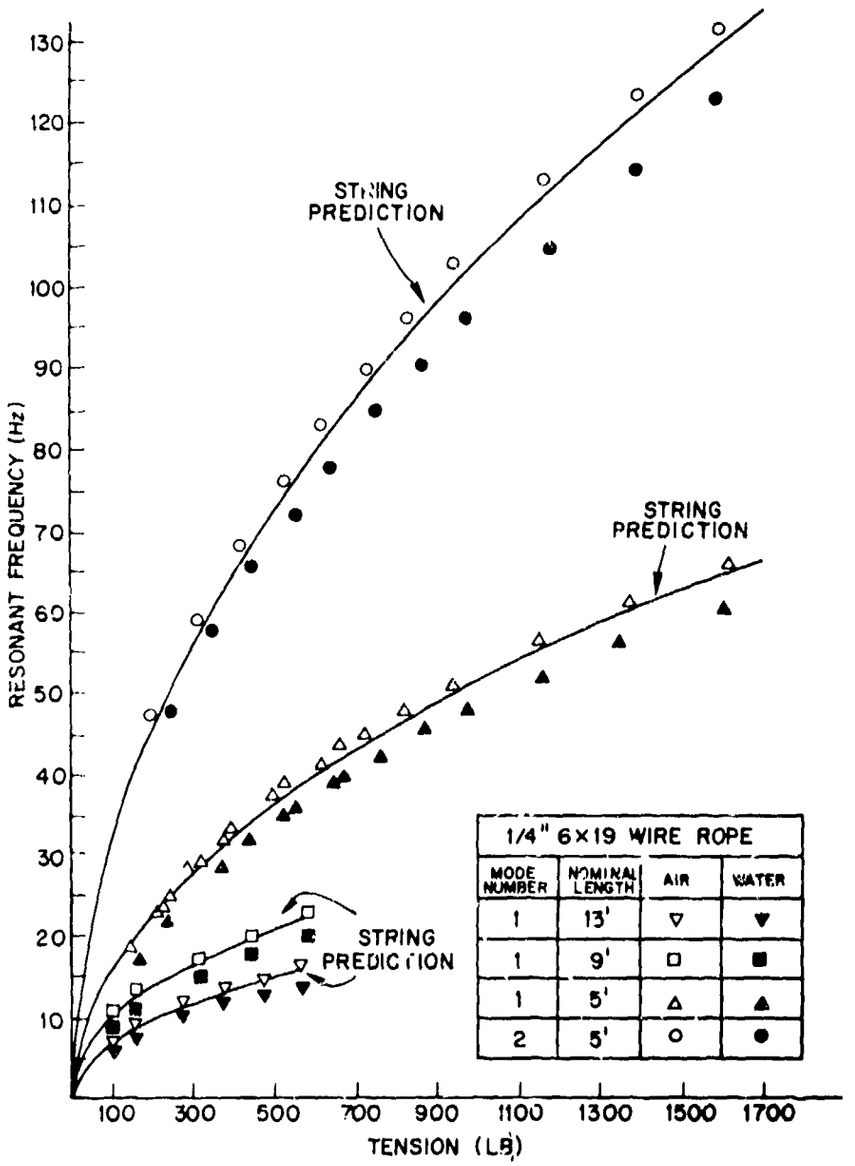

Fig. 4 Measured and predicted resonant frequencies of 1/4 in. diameter 6 x 19 wire rope specimens

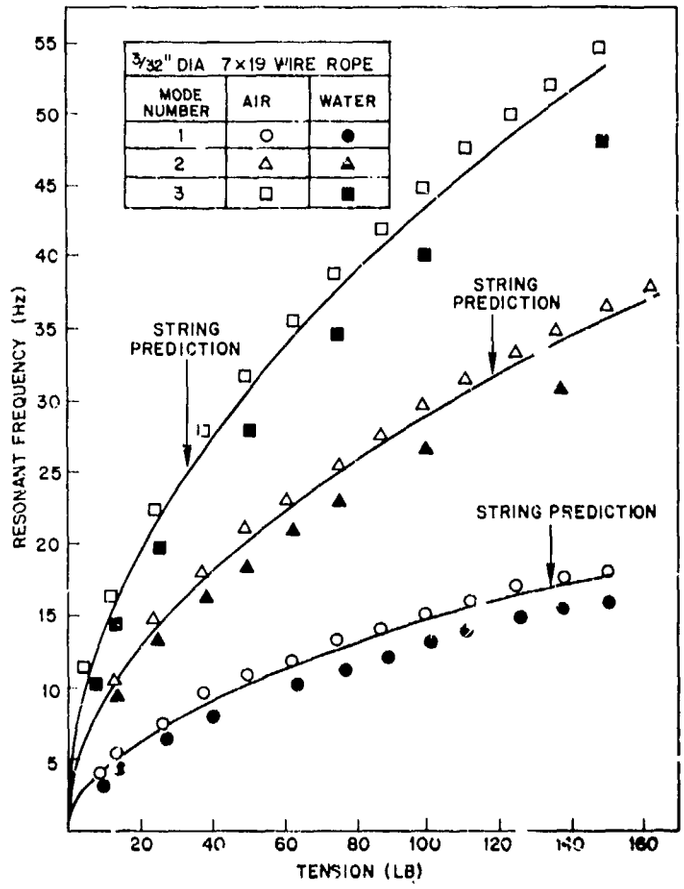

Fig. 5 - Measured and predicted resonant frequencies of 3/32 in. diameter 7 × 19 wire rope specimens

These observations are verified in Fig. 6. Here the ratio f_A/f_W is plotted as a function of f_W for all of the data in Figs. 4 and 5 This ratio, which is related to the virtual mass, is a weak function of frequency over much of the range tested with a slight upward trend for decreasing frequency. The frequency ratio shows no dependence on mode shape or wavelength. Moreover, for the two different sizes of cables, the ratios at all amplitudes up to 100% of a diameter are indistinguishable within the accuracy of the experiments. Several points for a 3/8 in. diameter cable from the report by Heller and Chung [6] are included for comparison. A slight increase appears in f_A/f_W with increasing cable size (2-4% for a 4:1 increase in cable diameter), but this variation is within the bounds of experimental accuracy.

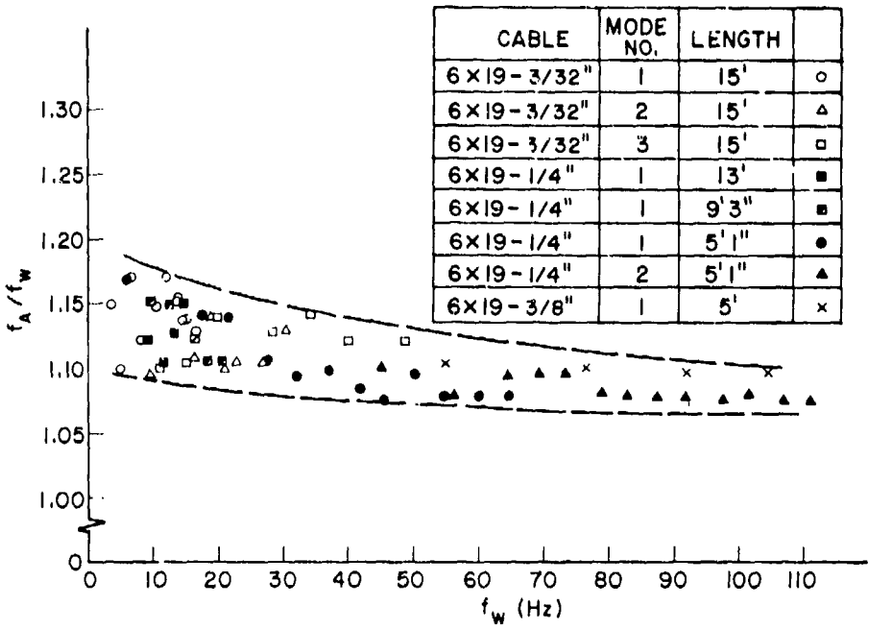

Fig. 6 — Ratio of in-air resonant frequency f_A to the in-water resonant frequency f_W as a function of f_W. The square of this ratio is equal to the ratio the virtual mass in water to the mass in air

The rather simple conclusion that the added mass is independent of amplitude, mode shape, and wavelength is not without precedent. King [10], in an experimental study of the added mass of flexible cylinders, has made the following conclusion:

> "It was shown that this 'added mass' effect was independent of frequency, amplitude, mode shape and streaming flow."

King's conclusion not only tends to confirm the results of this report but also serves to justify the application of added mass values obtained in still water to the situation where water is flowing about the cable causing it to oscillate.

The added mass coefficient K was calculated with Eq. (3) after passing a mean curve through the data in Fig. 6. The resulting curves are shown in Fig. 7 together with the 'probable mean line' of Heller and Chung [6]. The differences in the shape of 3/32 in. and 1/4 in. cable curves compared to the 3/8 in. cable could be a result of the error magnification inherent in Eq. (3), whereas the relative displacements in the curves are the result of a varying specific gravity. The measured values of specific gravities S are listed in the figure legend. Despite similarities in construction and materials of construction, the specific gravity increases with decreasing cable size. To see if air trapped between the larger strands of the larger cables was responsible, several cable specimens were immersed

in water and the container was evacuated. There was a slight increase in specific gravity, but it was not sufficient to account for the changes in S between cable sizes. To avoid this ambiguity and the introduction of yet another empirical quantity it is recommended that the virtual mass be computed directly from Eq. (2) in the form

$$\rho_W = \left(\frac{f_A}{f_W}\right)^2 \rho_A$$

where the frequency ratio is obtained from Fig. 6. In this way the virtual mass, which is the desired result, can be determined to within a reasonable variation of about ± 5%.

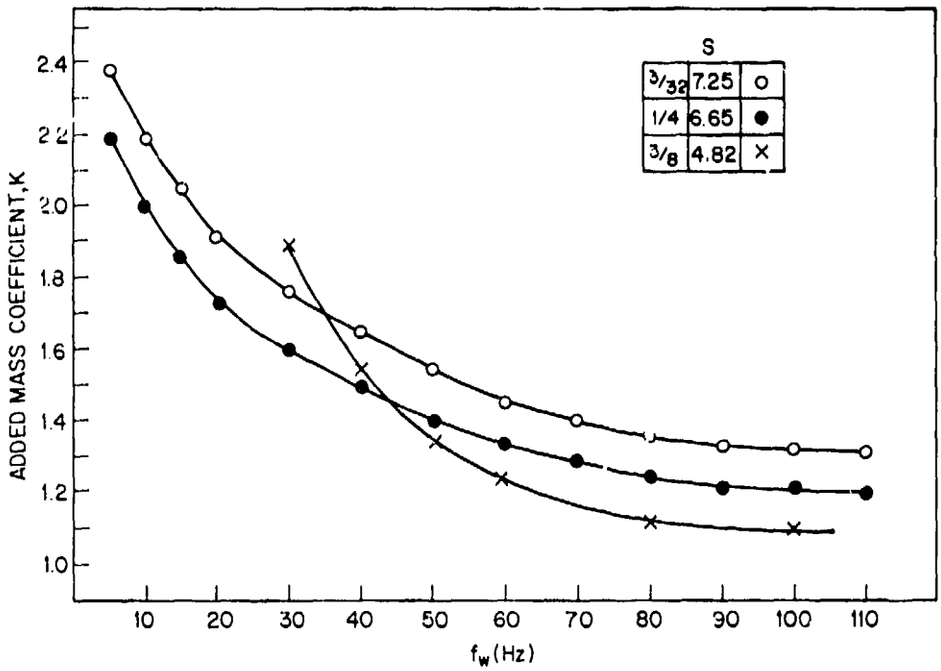

Fig. 7 — The added mass coefficient K

Since the added mass appears to be independent of wavelength, the theoretical added mass coefficient for a rigid cylinder serves as a useful comparison. The expression for this coefficient is [11]

$$K = 1 + 2\sqrt{2/R}\,, \quad R = \frac{\omega D^2}{4\nu} \tag{16}$$

where R is the vibration Reynolds number based on the cable diameter D, ω is the vibration frequency, and ν is the fluid kinematic viscosity. As can be seen from the values of R given in Table 1, the predicted values of K fall below the measured values for all cases

including the 3/8 in. cable data of Heller and Chung [6]. This is in conflict with Fig. 6 of their report, which shows good agreement between a predicted curve and the measured "probable mean" curve beyond 100 Hz.

To facilitate a comparison between measured and predicted resonant frequencies, a best fit according to

$$f_A = a_0 + a_1 \sqrt{T_0} \tag{17}$$

was obtained for the in-air resonant frequencies. A listing is given in Table 2 of the curve fit and predicted coefficients a_0 and a_1, as well as the standard deviation σ and the ratio of f_A/f_S for all configurations. The results in this table are intended to serve as a validation for the equivalent homogeneous string model and to give a quantitative measure of the accuracy of that model. During the experiments the tension was often sufficiently low to have a small amount of "sag" in the cable. However, the weight of the cable specimens never exceeded 5% of the applied tension, and so it is likely that nonlinear effects due to very slack or catenary cables were absent.

CABLE DAMPING

The overall damping at resonance will in general be a result of energy dissipation through the combined effects of internal and interstrand friction, radiation, transmission to the supports, and viscous losses in the surrounding fluid. Moreover the overall damping could likely be a function of frequency, amplitude, mode shape or wavelength within each medium. The functional dependence of the overall damping was determined from the experiments, but no attempt was made to partition the dissipated energy and, further, negligible losses were assumed at the supports. If the damping is dependent on amplitude but is small in magnitude then difficulty is introduced only into the damping term itself. The damping was in fact a function of amplitude during the initial experiments in air. Yu [12] has suggested that the damping mechanism of a stranded cable in air with no axial load is primarily interstrand friction. The interstrand friction depends on the contact forces, which are a function of the amplitude (local tension) and the equilibrium tension itself. The damping measurements in water did not exhibit amplitude or tension dependence since external losses greatly overshadowed the internal losses, and so the investigation of the in-air damping of cables was discontinued. The in-water log decrements for all configurations are presented as a composite in Fig. 8. It is evident from the results in the figure that the decrement is independent of wavelength and mode number, and that the decrease in decrement at higher modes is therefore principally a result of the higher frequency. This implies that the product δf must be constant or nearly so. Generally, the computed values of δf increased slightly with increasing frequency. For the 3/32 in. cable δf increased about 20% for an order of magnitude change in frequency, while for the 1/4 in. cable δf increased approximately 10%. It is worth noting that $\delta f \sim \beta$, the damping coefficient, so that the damping coefficient in water is independent of amplitude, wavelength and mode shape for the range of parameters tested. Furthermore, the damping coefficient is only slightly dependent on frequency.

Table 2
Comparison of Measured and Predicted Resonant Frequencies

Cable	Nominal Length (ft)	Mode Number	Curve Fit Results, f_A			String Prediction, f_S		f_A/f_S
			a_0	a_1	σ	a_0	a_1	
3/32 in. diameter 7 × 19	15	1	0.17	1.49	0.14	0	1.45	$1.027 + 0.12/\sqrt{T}$
	15	2	-0.32	3.01	0.19	0	2.90	$1.038 - 0.11/\sqrt{T}$
	15	3	0.58	4.44	0.17	0	4.35	$1.020 + 0.13/\sqrt{T}$
1/4 in. diameter 6 × 19	5	1	-0.08	1.67	0.97	0	1.65	$1.012 - 0.05/\sqrt{T}$
	5	2	1.30	3.34	2.5	0	3.30	$1.012 + 0.4/\sqrt{T}$
	9	1	0.83	0.95	0.79	0	0.93	$1.021 + 0.88/\sqrt{T}$
	13	1	0.33	0.68	0.31	0	0.67	$1.014 + 0.48/\sqrt{T}$

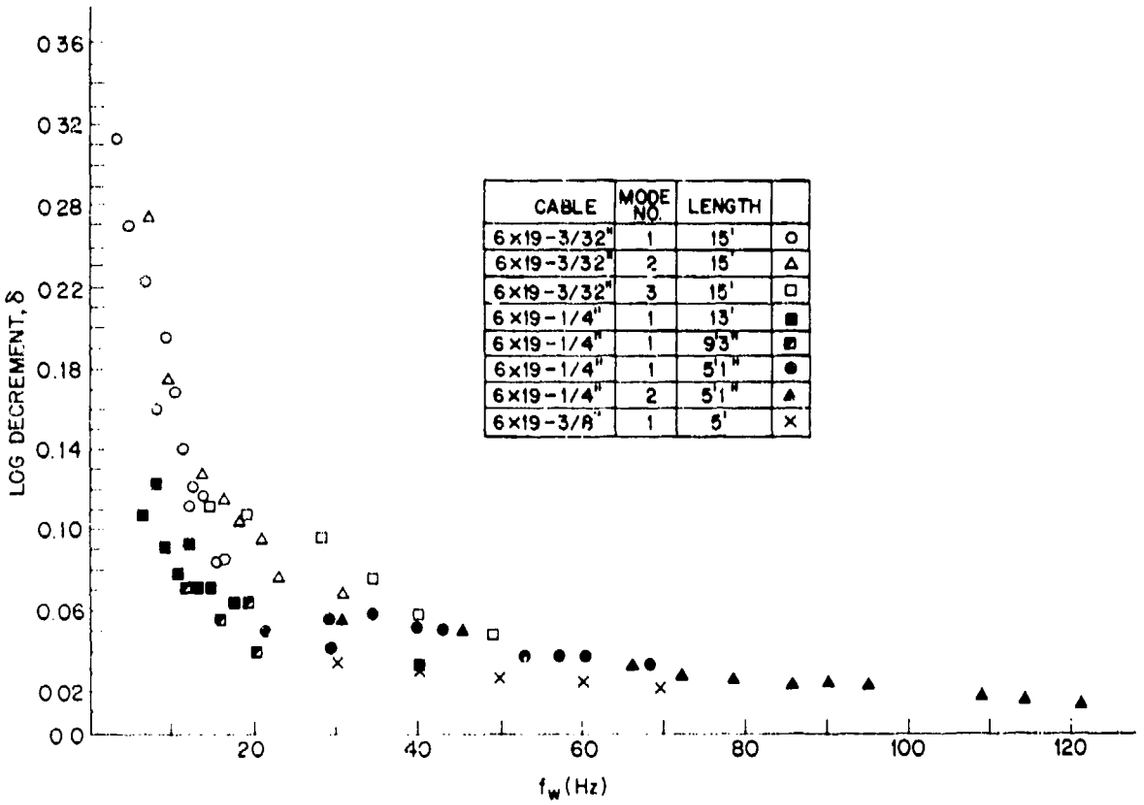

Fig. 8 - The log decrement of the free vibrations of a flexible cable in water

A similar result for a length of piano wire in air was published by Leehey and Hanson [13] in a paper that considered the sound radiation from a resonantly vibrating wire. From that paper, the damping quality factor, $Q = 2\pi/\delta$, of the first four modes of a piano wire yields essentially the same value when divided by the corresponding resonant frequency. Both the quality factor Q and the quotient $Q/f = 2\pi/\delta f$ are listed in Table 3 for comparison purposes.

Table 3
The Damping Characteristics Of A Piano Wire*

Mode Number	Frequency (Hz)	$Q = 2\pi/\delta$	$Q/f = 2\pi/\delta f$
1	470	515	0.91
2	923	920	1.00
3	1387	1387	1.00
4	1683	1950	0.96

*From Leehey and Hanson [13].

Once again a comparison can be made with the results of Heller and Chung [6]. Several representative data points from Chung's dissertation [9], for a 6 × 19, 3/8 in. diameter wire rope, are plotted in Fig. 8. There is good agreement on the effects of frequency and the suggestion of a diameter effect for the three cable sizes. Attempts to collapse the damping data onto a single curve using the vibration Reynolds number were not successful because of the several loss mechanisms that contribute to the overall damping of a cable during transverse vibrations in water.

APPLICATION OF THE RESULTS TO FLOW-INDUCED CABLE VIBRATIONS

In the absence of Reynolds number and Froude number effects, the amplitude x of a cylindrical structure undergoing vortex-excited oscillations can be expressed as a function of certain parameters,

$$x = f(f_n, M, D, \delta, V, \rho), \tag{18}$$

where

f_n = natural frequency

M = body mass plus added mass (virtual mass) per unit length

δ = logarithmic decrement of damping

D = body diameter

V = free stream fluid velocity

ρ = fluid density. Dimensional analysis leads to the following nondimensional parameter groupings:

$$\frac{x}{D} = f\left(\frac{V}{f_n D}, \frac{M}{\rho D^2}, \delta\right). \tag{19}$$

Vickery and Watkins [14] have shown that two of these groups can be combined into a single parameter (called a combined stability parameter),

$$k_s = \left(\frac{2M}{\rho D^2}\right)\delta, \tag{20}$$

when the energy dissipated by damping at resonance is equated to the energy input from fluid forces. Griffin, Skop, and Koopmann [3] have shown that the equations of NRL's wake-oscillator mathematical model lead to another form of the combined stability parameter,

$$\frac{\zeta}{\mu} = 2\pi S^2 k_s, \tag{21}$$

where S is the Strouhal number, ζ is the damping coefficient $\delta/2\pi$, and μ is a mass parameter,

$$\mu = \frac{\rho D^2}{8\pi^2 S^2 M} . \tag{22}$$

Since the Strouhal number $S = f_s D/V$ (f_s is the vortex-shedding frequency from a stationary body) is constant over the practical range of vortex shedding, the two forms of the combined stability parameter are linearly related.

It has further been shown that the peak amplitude of resonant vortex-excited oscillation of an elastically-mounted, rigid cylinder of flexible cylinder is only a weak function of $V/f_n D$, with the peak value of amplitude in the transverse, or crossflow, direction to the incident current generally occurring in the range

$$\frac{V}{f_n D} = 5.5 \text{ to } 6.5 .$$

Thus the peak amplitude of vortex-excited oscillation is a function of only the combined stability parameter as shown in Fig. 9 where experimental data from NRL and elsewhere are plotted together with a predicted curve generated with the wake-oscillator model [3].

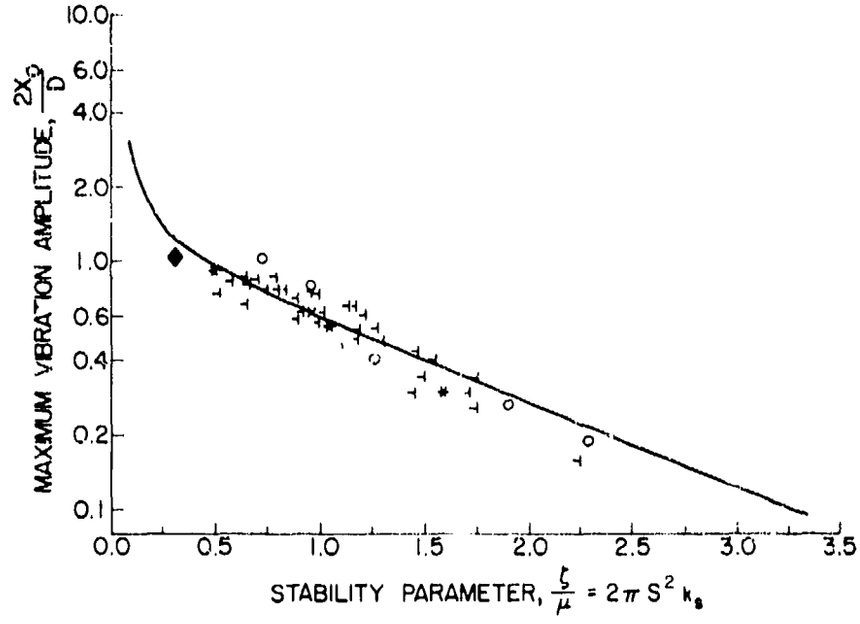

Fig. 9 — The maximum amplitude of vortex-excited oscillation for a rigid, elastically mounted cylinder. Experimental data (air): NRL, +; University of British Columbia, O ●; University of Maryland, ·. Experimental data (water): University of Padua, ♦. The prediction of the NRL wake-oscillator model [3] is denoted by the solid line.

For values of ζ/μ greater than about 3.4 to 4.0, the amplitude of oscillation falls below $2x_0/D = 0.10$, which is the threshold usually associated with the onset of resonant, vortex-excited oscillations. The interesting and practical result indicated by the figure is that beyond a critical, or cutoff, value for the stability parameter, vortex-excited resonant oscillations do not occur. A combination of structural and flow properties which combine to yield a value of ζ/μ such that

$$\frac{\zeta}{\mu} > \frac{\zeta}{\mu}\Bigg)_{\text{critical}}$$

characterize a system that will not resonantly vibrate under vortex excitations. Such behavior has been observed for both flexible cylinders [15] and elastically mounted rigid pendulum structures in both air and water [14], which suggests that an equivalent combined stability parameter ζ/μ or k_s can be specified for a strumming underwater cable once the damping and added mass have been determined.

The natural modes of the cable vibrations can be determined from the frequency law for a stretched string

$$f_n = \frac{j}{2L}\sqrt{\frac{T}{M}}, \quad j = 1, 2, 3 \ldots .$$

where L is the cable length, T is the tension, and $M = \rho A$ is the mass per unit length. The virtual mass in water can be deduced from the ratio of the natural frequencies in air and water at corresponding values of tension and wavelength. This ratio of natural frequencies is plotted in Fig. 6 as a function of the natural frequency f_W. A typical virtual mass computation at $f_W = 20$ Hz is given by

$$\frac{M_W}{M_A} = \left(\frac{f_A}{f_W}\right)^2 = (1.13)^2 = 1.28 , \tag{23}$$

which represents a 28% increase in the apparent mass in water from the in-air value.

These results can be used to determine the combined stability parameter k_s for the strumming vibrations of cables as shown in Table 4. The strumming response of the cable was measured by Dale, et al. [16]. The cable lengths for the experiment were 3 and 6 ft and the cable diameter was 0.1 in. ($D \approx 3/32$ in.). Thus the cable damping and added mass results for the 0.1 in. cable in Figs. 5 and 7 can be used to compute k_s. The four values of frequency in Table 4 correspond to resonant strumming vibrations in the second through fourth modes for the 3-ft cable and the fourth through ninth modes for the 6-ft cable. It is interesting to note the decrease in k_s and ζ/μ as the frequency increases; this is a result of the decrease in the cable damping as the natural frequency is increased from 10 to 30 Hz in Fig. 7. The values of k_s in Table 4 correspond to a range of peak-to-peak, resonant strumming amplitudes between 1 and 3 diameters [3,16].

Table 4
The Damping Characteristics of Strumming Cables

Frequency[1], f_W (Hz)	Combined Stability Parameter[2]	
	$k_s = \left(\frac{2M}{\rho D^2}\right)\delta$	$\frac{\zeta}{\mu} = 2\pi S^2 k_s$
31	0.56	0.15
28	0.80	0.22
21	1.20	0.33
14	1.60	0.44

[1]Frequency data from Dale et al [16]. Cable diameter = 0.1 in., cable length = 6 ft, 3 ft.
[2]Cable damping and virtual mass from Figs. 5 and 7. Cable specific gravity = 7.25.

CONCLUSIONS

The equivalent homogeneous string is an adequate representation of the transverse vibration of stranded wire rope for peak-to-peak amplitude of vibration up to at least a full cable diameter. For tensions between 1 and 60% of the cable rupture strength the predicted resonant frequency in air will be 1-4% below the actual natural frequency.

The added mass effect in water is independent of amplitude (up to 100% of a diameter), mode shape, wavelength, and is only slightly dependent on frequency. The virtual mass is most conveniently and accurately determined from

$$\rho_W = \left(\frac{f_A}{f_W}\right)^2 \rho_A$$

where the ratio f_A/f_W is obtained from Fig. 5 of this report.

The damping or log decrement δ of free vibrations in water at resonance is also independent of amplitude (up to 100% of a cable diameter), mode shape, and wavelength. In addition, the damping coefficient β increases very little with frequency so that the log decrement is, to a good approximation, inversely proportional to frequency.

The damping and added mass can be combined to form a "stability parameter" that governs the onset and magnitude of vortex-induced cable vibrations. This stability parameter can be used to estimate correctly the maximum amplitude of transverse motion at the antinode of a vibrating, flexible cable.

REFERENCES

1. S.E. Ramberg and O.M. Griffin, "Vortex Formation in the Wake of a Vibrating, Flexible Cable," accepted by Trans. ASME, J. Fluids Eng.

2. S.E. Ramberg and O.M. Griffin, "Velocity Correlation and Vortex Spacing in the Wake of a Vibrating Cable," accepted by Trans. ASME, J. Fluids Eng.

3. O.M. Griffin, R.A. Skop, and G.H. Koopmann, "The Vortex-Excited Resonant Vibrations of Circular Cylinders," J. Sound Vib. **31** 235-249 (1973).

4. F.O. Ringleb, "Motion and Stress of an Elastic Cable due to Impact," J. Appl. Mech. **24**, 417-425 (1957).

5. W. Li, "Elastic Flexible Cable in Plane Motion under Tension," J. Appl. Mech. **81** 587-593 (1959).

6. S.R. Heller and B.S. Chung, "On the Transverse Vibration of Wire Rope," Catholic University of America Report 72-7, Washington, D.C., 1972.

7. S.R. Heller, private communication, 1974.

8. G.S.S. Murthy and B.S. Ramakrishna, "Nonlinear Character of Resonance in Stretched Strings," J. Acoust. Soc. Amer. **38**, 461-471 (1965).

9. B.S. Chung, "Dynamic Properties of Selected Wire Ropes Subjected to Axial Loads," (Ph.D. Dissertation, Catholic University of America, 1971).

10. R. King, "The 'Added Mass' of Cylinders," British Hydromechanics Research Association, BHRA Report TN1100, 1971.

11. L. Rosenhead, ed., *Laminar Boundary Layers*, Oxford University Press, London, 1963, pp. 390-393.

12. A. Yu, "Vibration Damping of Stranded Cable," Proc. Soc. Exp. Stress Anal. **IX**, No. 2, 141-158 (1952).

13. P. Leehey and C.E. Hanson, "Aeolian Tones Associated with Resonant Vibration," J. Sound Vib. **13**, 465-483 (1971).

14. B.J. Vickery and R.D. Watkins, "Flow-Induced Vibrations of Cylindrical Structures" *Proceedings of the First Australasian Conference of Hydromechanics*, 1962 in University of Western Australia.

15. R. King, M.J. Prosser, and D.J. Johns, "On Vortex Excitation of Model Piles in Water," J. Sound Vib. **29** 169-188 (1973).

16. J. Dale, H. Menzel, and J. McCandless, "Dynamic Characteristics of Underwater Cables Flow-Induced Transverse Vibrations," U.S. Naval Air Development Center Report NADC-AE-6620, 1966.